RSC Advances

PAPER

View Article Online
View Journal | View Issue

Cite this: *RSC Adv.*, 2023, **13**, 13269

Engineering S-scheme CuO/ZnO heterojunctions sonochemically for eradicating RhB dye from wastewater under solar radiation

Ali Alsulmi,[a] Nagy N. Mohammed,[b] Ayman Soltan,[bc] M. F. Abdel Messih[b] and M. A. Ahmed*[b]

Received 10th February 2023
Accepted 10th April 2023

DOI: 10.1039/d3ra00924f

rsc.li/rsc-advances

In this research, S-scheme heterojunctions composed of different concentrations of CuO and ZnO nanoparticles are fabricated for eradicating rhodamine B dye under solar radiation. ZnO nanoparticles are designed through a facile sol–gel route employing Triton X-100. Spherical CuO nanoparticles of 15.2 nm and 1.5 eV band gap energy are deposited on ZnO nanoparticles in an ultrasonic bath of 300 W intensity. The physicochemical performance of the photocatalyst is explored by HRTEM, SAED, BET, XRD, DRS and PL. The *in situ* homogeneous growth of spherical CuO nanoparticles on ZnO active centers shifts the photocatalytic response to the deep visible region and enhances the efficiency of charge carrier separation and transportation. Among all heterojunctions, ZnCu10 containing 10 wt% CuO displays the best photocatalytic rate for expelling 93% of RhB dye within 240 min, which is twenty-fold higher than that of pristine ZnO and CuO. Reactive oxygen species are the predominant species in degrading the dye pollutant on the heterojunction surface, as shown from scrubber trapping experiments and PL spectrum of terephthalic acid. Coupling ZnO as an oxidative photocatalyst and CuO as a reductive photocatalyst generates an efficient S-scheme heterojunction with strong redox power in destructing various organic pollutants.

1. Introduction

Organic pollutants emerging from the textile, dyestuff and cosmetic industries are dangerous threats to human health and aquatic life.[1–5] These organic pollutants possess a stable aromatic structure that resists decomposition by traditional routes or biological treatment.[5–10]. To tackle the shortcoming of the traditional routes, photocatalysis employing low cost semiconductors and solar radiation provide an auspicious route for complete destruction of organic pollutants. MoO_3, ZnO, MnO_2, TiO_2, CeO_2 and SnO_2 nanoparticles degrade various organic dyes under UV light irradiation.[11–16]. In particular, ZnO is a biocompatible, non-toxic and cost-effective starting material for generating a huge amount of reactive oxygen species and hot charge carriers that expel organic pollutants from wastewater.[17–28] The poor solar radiation absorbability, fast electron–hole recombination and slow charge transportation restrict the photocatalytic reactivity of ZnO. To tackle the shortcoming of ZnO single photocatalyst, a heterojunction composed of two different semiconductors with an aligned band gap structure is paid more attention in recent years. The charge carrier diffusion across the interface boundary between the two semiconductors is investigated by different electronic mechanisms. The traditional routes such as straddling type I, staggered type (II) and all types of Z-scheme fail in scrutinizing the direction of electron–hole migration. The S-scheme mechanism is an auspicious novel aspect for exploring the real direction of charge transportation through the heterojunction circuit under solar light illumination.[29–40]. The heterojunction is composed of oxidative and reductive photocatalysts with different work functions and Fermi level positions.[41,42] The main universal condition requires that the Fermi level and conduction band position of the reductive photocatalyst be higher than those of the oxidative photocatalyst. When the two semiconductors approach each other, the electrons of the reductive photocatalyst transfer to the oxidative photocatalyst. The Fermi levels of the oxidative and reductive photocatalysts bend upward and downward, respectively, until the two levels are equilibrated. At this contact point, the holes of the reductive photocatalyst and electrons of the oxidative photocatalyst are recombined and vanished by coulombic electrostatic force. On the contrary, the positive holes of the oxidative photocatalyst and electrons of the reductive photocatalyst with strong redox power are consumed in the photocatalytic reaction. Coupling CuO with ZnO nanoparticles is promising for constructing a successful heterojunction for driving the photocatalytic response to the visible region, decreasing the rate of electron–hole coulombic

[a]*Department of Chemistry, College of Science, King Saud University, Riyadh, Saudi Arabia*

[b]*Department of Chemistry, Faculty of Science, Ain Shams University, Abbassia, Cairo 11566, Egypt. E-mail: abdelhay71@hotmail.com; Fax: +20 224831836; Tel: +20 103979568*

[c]*Department of Chemistry, University of York, York YO10 5DD, UK*

attraction force and increasing the lifetime of the charge carriers compared with pristine ZnO and CuO nanoparticles.[43–53] Zare *et al.* prepared CuO/ZnO and Ag/CuO/ZnO through a quick co-precipitation method for photodegradation of methylene blue dye.[43] The experimental results reveal the successful degradation of MB dye due to the role of Ag and CuO in limiting the rate of electron–hole attraction. Ruan *et al.* synthesized CuO/ZnO by a microwave assisted route for mitigation of acid orange 7 dye. The decomposition of 80% of the toxic dye results from strong charge transportation *via* the direct Z-scheme mechanism.[44] Hussain *et al.* prepared CuO/ZnO/MoO_3 by a hydrothermal method for effective destruction of 97% of RhB dye. The superior reactivity of the ternary system is attributed to the matching in band gap structure of the heterojunction constituents.[45] Wang *et al.* prepared CuO/ZnO nanowires by a thermal oxidation method for successful decomposition of MB dye. The experimental results reflect that the nanocomposite exhibits both photocatalytic and super-hydrophobic features.[46] Fouda *et al.* synthesized CuO/ZnO through a green biosynthesis method for effective destruction of 97% of MB under visible light. The experimental work supports that introduction of CuO reduces the crystallite size of the nanocomposite, which enhances the photocatalytic performance.[47] Mendoza *et al.* recorded the high dispersion of CuO nanoparticles on the ZnO surface enriched with hydroxyl groups synthesized by a simple impregnation method for exceptionally eradicating MB dye from aqueous solution.[48] Harish *et al.* recorded that aggregation of CuO nanoparticles during the photocatalytic reaction reduces the efficiency of the solid catalyst due to the pronounced drop in the specific surface area and the number of active sites.[49] Singh *et al.* prepared CuO/ZnO decorated with Ag nanoparticles by a combined hydrothermal and chemical reduction route for photocatalytic decomposition of rhodamine 6G dye. The experimental results imply that incorporation of various concentrations of silver increases the decomposition of the dye from 40% over CuO–ZnO to 90% over Ag/ZnO–CuO due to the influence of silver in increasing the lifetime of the charge carriers.[50] Cao *et al.* prepared novel tree-like ZnO/CuO composites by thermal oxidation and hydrothermal routes for photodegradation of rhodamine dye. The existence of Cu foam supplies a large surface area for the growth of tree-like CuO/ZnO composites and acts as an effective frame to support the catalysts.[51] Engineering CuO/ZnO heterojunctions through traditional operations such as precipitation, hydrothermal, microwave and thermal oxidation processes is energy consuming and requires vigorous operating conditions, which presumably deteriorate the metal oxide structure. The sonochemical route is an efficient, fast and green process for engineering heterojunctions with strong chemical interactions between their constituents. The sonochemical process is triggered by ultrasonic irradiation that generates various bubbles, cavities, shock waves and micro-jets in the reaction medium within few microseconds. These phenomena enhance the chemical interaction between the nuclei of ZnO and CuO to generate a successful heterojunction. In this novel research, S-scheme CuO/ZnO heterojunctions are well engineered with various concentrations of CuO and ZnO through the sonochemical route for photocatalytic mitigation of rhodamine B dye. The heterojunctions are vividly investigated by XRD, HRTEM, SAED, DRS, PL and BET techniques. The photocatalytic efficiency of the heterojunction is well explored and compared by following the mitigation of rhodamine B under solar radiation. Scrubber trapping experiments and PL analysis of terephthalic acid were executed quantitatively to determine the type of reactive oxygen species that is responsible for expelling RhB dye. This research work shed light on engineering S-scheme heterojunctions of low cost and strong redox power for expelling various organic dyes from wastewater.

2. Materials and methods

2.1. Materials

Zinc acetate, Triton X-100, copper sulphate, sodium hydroxide, absolute ethanol, RhB dye, ammonium oxalate, isopropanol, benzoquinone and terephthalic acid are obtained from Sigma-Aldrich Company with purity = 99%.

2.1.1. Preparation of ZnO nanoparticles. 12 g of zinc acetate with high purity is dissolved in distilled water with constant stirring for one hour. An appropriate amount of Triton X-100 is added with vigorous stirring for three hours to the above solution. Afterwards, 1 M ammonia solution is added dropwise to the above mixture to generate a milky zinc hydroxide sol. Subsequently, the sol mixture is agitated for 6 hours under ambient conditions. The total mixture is transferred to a dark box and left for gelation for 5 days. A brilliant white gel is generated after aging. Successive washing with hot distilled water is introduced to eradicate any extra ions in the solution medium. The wet gel is dried at 90 °C overnight for excluding physisorbed ammonia and water. The dried solid is finally annealed at 350 °C at a rate of 5 °C min^{-1} for six hours. Finally, ZnO nanoparticles are collected and ground in a porcelain mortar and sieved to collect fine nanoparticles with auspicious photocatalytic properties.

2.1.2. Preparation of CuO nanoparticles. 15.3 g of $CuSO_4$ is dissolved in distilled water, followed by addition of a defined amount of Triton X-100 with vigorous stirring for three hours. 1 M sodium hydroxide is added drop by drop to the above solution and the pH is adjusted at pH = 9. The brilliant bluish precipitate of copper hydroxide suspended in the aqueous solution is agitated for three hours with a constant rate. The solution mixture is left for five days to spontaneous sol–gel transformation. The collected gel particles are purified using a simple filtration system and washed several times with distilled water to remove sulphate and sodium ions. The wet gel is dried at 80 °C and annealed at 400 °C for five hours. The resultant black solid is cooled to ambient temperature overnight. The annealed solid is collected and ground carefully in a porcelain mortar to homogenize the solid matrix without destroying the crystalline structure.

2.1.3. Preparation of CuO/ZnO heterojunctions. Typically, CuO/ZnO nanoparticles are synthesized through a low cost sonochemical route. Various proportions of CuO and ZnO nanoparticles dispersed in distilled water are mixed by certain proportions to obtain 5, 10 and 15 wt% CuO/ZnO. Each of the above mixture is subjected to an ultrasonic bath of 300 W intensity for 40 minutes to enhance the chemical deposition of CuO on the ZnO surface. Then, the sol mixture is filtered and dried at 100 °C for 24 hours. Finally, the collected solid

specimen is ground in a porcelain mortar carefully to avoid sample deterioration and stored in a Falcon tube. The photocatalysts are denoted as ZnO, CuO, ZnCu5, ZnCu10, and ZnCu15 for pristine ZnO, CuO and the heterojunctions containing 5, 10 and 15 wt% CuO, respectively.

2.1.4. Photodegradation of rhodamine B dye. The photocatalytic decomposition of RhB dye under a solar simulator is investigated on the surface of pristine ZnO and CuO as well as the heterojunctions. Typically, 0.1 g of the photocatalyst is dispersed in a glass reactor with 100 ml of 2×10^{-5} M RhB dye solution and the mixture is stirred vigorously with a rate of 300 rpm under dark conditions for one hour to achieve the adsorption–desorption equilibrium. Then, a solar simulator with an intensity of 300 W is switched on the above mixture for four hours. At different interval times, 4 ml of the solution mixture is taken out, centrifuged, and analyzed using a UV-visible spectrophotometer.

2.2. Material characterization

A PANalytical X'PERT MPD diffractometer with Cu [$K\alpha_1/K\alpha_2$] radiation is employed to investigate the crystalline properties of the as-synthesized heterojunctions. The diffraction angle ranges from 10° to 90° with a step of 0.02° and integration time of 3 (s per step). The pore structure and surface area of the solid specimens are explored by adsorption isotherms of N_2 gas on the photocatalyst surface at 77 K. A high resolution transmission electron microscope HRTEM JEOL 6340 elaborates the nanostructure and size of the as-synthesized photocatalyst. The diffuse reflectance spectrum was recorded using a JASCO spectrometer (V-570) for exploring the optical properties of the solid specimens. A Lumina fluorescence spectrometer (Thermo Fisher Scientific) elaborates the separation efficiency of the photogenerated electron–hole pairs. A Shimadzu UV-visible spectrophotometer is employed to determine the change in color intensity of RhB in the wavelength range (200–800) nm.

3. Results and discussion

3.1. Physicochemical characterization

XRD patterns of ZnO, CuO, ZnCu5 and ZnCu10 are well represented in Fig. 1 to investigate, with precise analysis, the dispersion of ZnO and CuO crystalline phases with respect to each other. Sharp characteristic peaks are detected at $2\theta = 31.66$, 34.28 and 36.22 corresponding to the (100), (002) and (101) planes of the wurtzite structure of ZnO (JCPDS card no. 79-0208). The diffraction peaks of CuO single phase are detected at $2\theta = 32.4$, 35.48° and 38.78° referred to the (110), (−111) and (111) diffraction planes of monoclinic CuO nanoparticles (JCPDS card no. 89-2529). The diffraction patterns of ZnCu5 and ZnCu10 show diffraction peaks assigned to both ZnO and CuO, revealing the coexistence of both semiconductor phases with different relative intensities dependent on the composition of each phase. The small shift of the diffraction peaks of ZnO and CuO to lower 2θ values is clearly observed. This shift in the diffraction peak positions can be ascribed to the substitution of Zn^{2+} by Cu^{2+} ions. The small difference in the ionic radius of Zn^{2+} (0.74 Å) and Cu^{2+} (0.73 Å) manifests that Cu^{2+} ions easily substitute Zn^{2+} ions. The crystalline dimensions detected by the Debye–Scherrer equation are 35.1, 15.4, 45.7 and 47.2 nm for ZnO CuO, ZnCu5 and ZnCu10, respectively.

Fig. 2 illustrates the adsorption–desorption isotherms of nitrogen at 77 K on pristine ZnO and the ZnCu10 heterojunction. The pore structure of ZnO and ZnCu10 is quantified by type II isotherm with H3 hysteresis loop, which referred to a slit pore structure. The surface areas of ZnO and ZnCu10 nanocomposites calculated from the BET equation are 25 and 18 $m^2\ g^{-1}$. The depression in heterojunction surface area results from strong deposition of CuO on the ZnO surface. This situation is further elaborated by HRTEM and XRD analysis, which illustrates the enlargement in the crystal dimension. The nanostructure and chemical dispersions of heterojunction constituents are further elaborated by HRTEM and the crystalline planes are well investigated by SAED analysis [Fig. 3]. A perfect hexagonal structure of wurtzite ZnO is recorded in Fig. 3a. The intimate contact of spherical CuO nanoparticles on the ZnO surface in auspicious arrangement without any agglomeration is illustrated in Fig. 3b. HRTEM implies the existence of lattice fringes of spacing 0.246 and 0.23 nm, ascribed to ZnO (101) and CuO (111) nanoparticles, respectively manifesting the successful construction of an S-scheme heterojunction [Fig. 3c]. SAED analysis of ZnCu10 shows various diffraction rings assigned to (100), (002) and (101) planes of hexagonal ZnO in addition to the (111) plane of monoclinic CuO nanoparticles [Fig. 3d]. The DRS spectrum is constructed for analyzing the optical properties, determining the band energy and elaborating the type of electronic transition of the as-synthesized samples. The spectrum displays an absorption band edge at 410 nm assigned to the traditional ZnO intrinsic absorption tendency [Fig. 4a]. The absorbability of ZnO directed its photocatalytic features under the UV region only, which restricts the industrial and environmental applications with solar energy. CuO exhibits a strong absorption band edge at 800 nm [Fig. 4b] resulting from its intensive black color, which provides a strong absorbability of CuO/ZnO heterojunctions in the deep visible region [Fig. 4c]. This phenomenon indicates that ZnO nanoparticles coupled with CuO can absorb readily solar energy with excellent photocatalytic performance. The band gap energy calculated from the Tauc equation is 3.05, 1.5 and 1.7 for ZnO, CuO and ZnCu10, respectively [Fig. 4d–f]. The PL emission characteristics of ZnO, ZnCu5 and ZnCu10 nanoparticles are measured at an excitation wavelength of 350 nm [Fig. 5]. The emission signal is reduced with introducing 5 and 10 wt% CuO nanoparticles, implying the reduction in the rate of electron–hole coulombic attraction force.

3.2. Photocatalytic degradation of RhB dye

Rhodamine B is an attractive cationic dye with an intensive florescent red color and stable aromatic structure. In the food and textile industries, RhB is the main component that provides the final product with stable color intensity under light irradiation. The strong chemical stability and complex aromatic structure restrict the destruction of RhB dye through traditional and biological routes. Photocatalytic destruction of RhB on

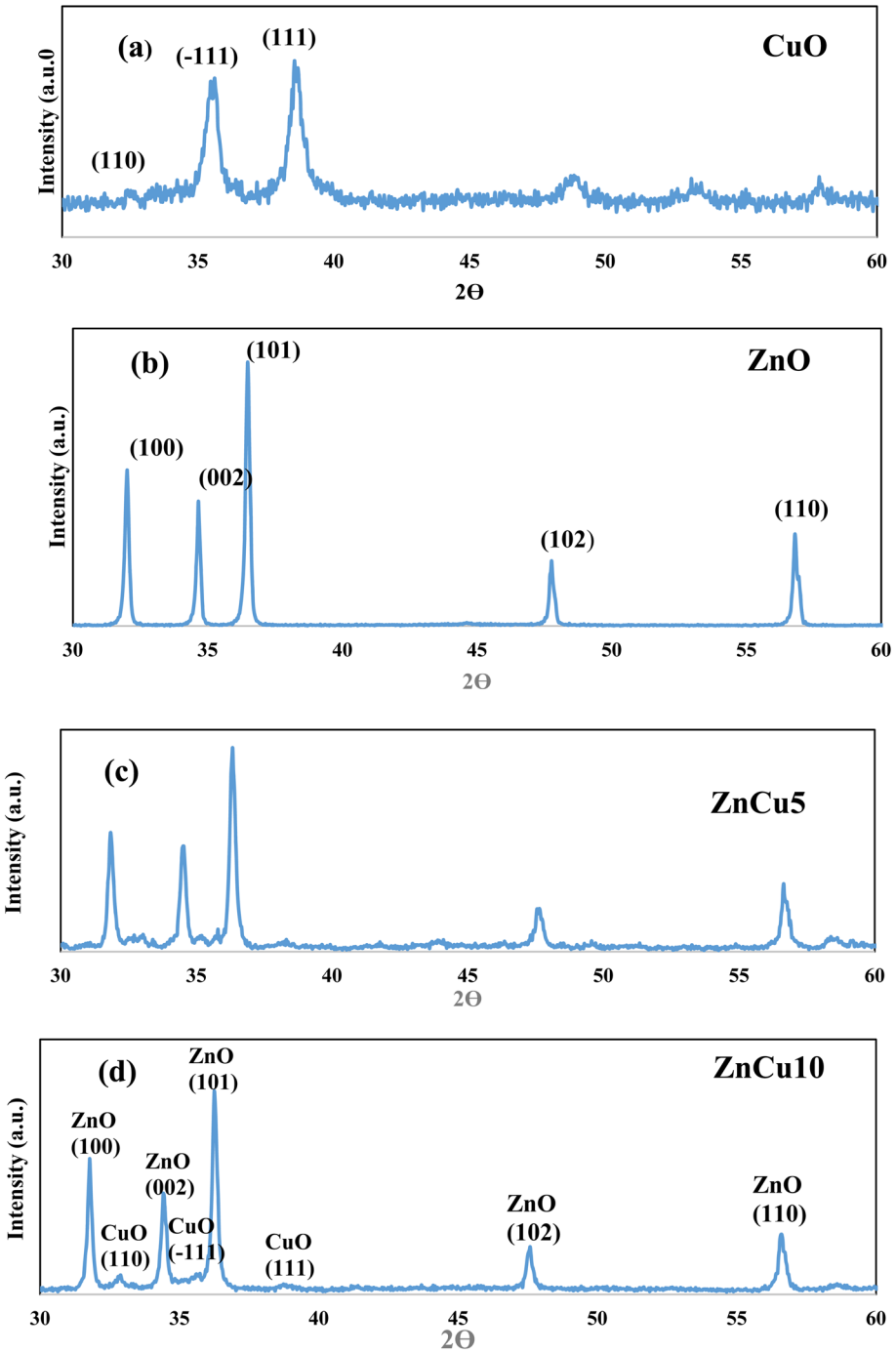

Fig. 1 XRD of (a) CuO, (b) ZnO, (c) ZnCu5 and (d) ZnCu10.

a suitable semiconductor surface under light irradiation is a promising route for wastewater remediation. Without a semiconductor, RhB is barely degraded and the amount of dye decomposed after 3 hours under light irradiation does not exceed 3% of the initial dye concentration. The photocatalytic performance of pristine ZnO and heterojunctions containing various concentrations of CuO (5–15) wt% is illustrated in Fig. 6. Pristine ZnO and CuO nanoparticles display very low reactivity in decomposing RhB under solar radiation due to the poor absorbability of ZnO nanoparticles and ultra-fast recombination rate of electron–hole pairs of CuO. Compared with pristine ZnO, all the heterojunctions with various concentrations of CuO display an auspicious reactivity in decomposing RhB dye [Fig. 6]. At the beginning of the photocatalytic reaction, 100 ml of dye solution is mixed with 0.1 g of the photocatalyst in a black box for one hour to estimate the adsorption capacity of the solid specimens. The concentration of dye degraded under adsorption–desorption aspects does not exceed 5% of the initial dye

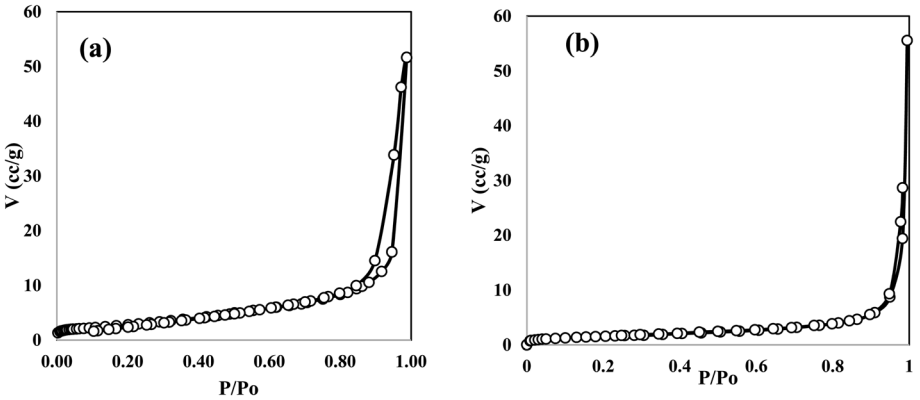

Fig. 2 N_2 adsorption–desorption isotherm of (a) ZnO and (b) ZnCu10.

concentration due to the low surface area of ZnO and CuO before and after mixing. Subsequently, on switching the visible light radiation, the reactive oxygen radicals are generated on the semiconductor surface, decomposing RhB dye into CO_2 and H_2O. The heterojunction composed of 5 wt% CuO and 95% ZnO degrades 90% of RhB dye compared with 18% removal on pristine ZnO. Increased ZnO loading with 10 wt% of CuO elevate the RhB decomposition to 93% [Fig. 7a]. Further loading ZnO with 15 wt% CuO reduces the efficiency to 31% due to the agglomeration of successive CuO screening layers that prevents the interaction between light irradiation and the photocatalyst surface. The pseudo first order rate constant for degrading RhB dye is 0.0003, 0.0003, 0.0066, 0.0067 and 0.0009 min^{-1} over the surface of ZnO, CuO, ZnCu5, ZnCu10 and ZnCu15, respectively

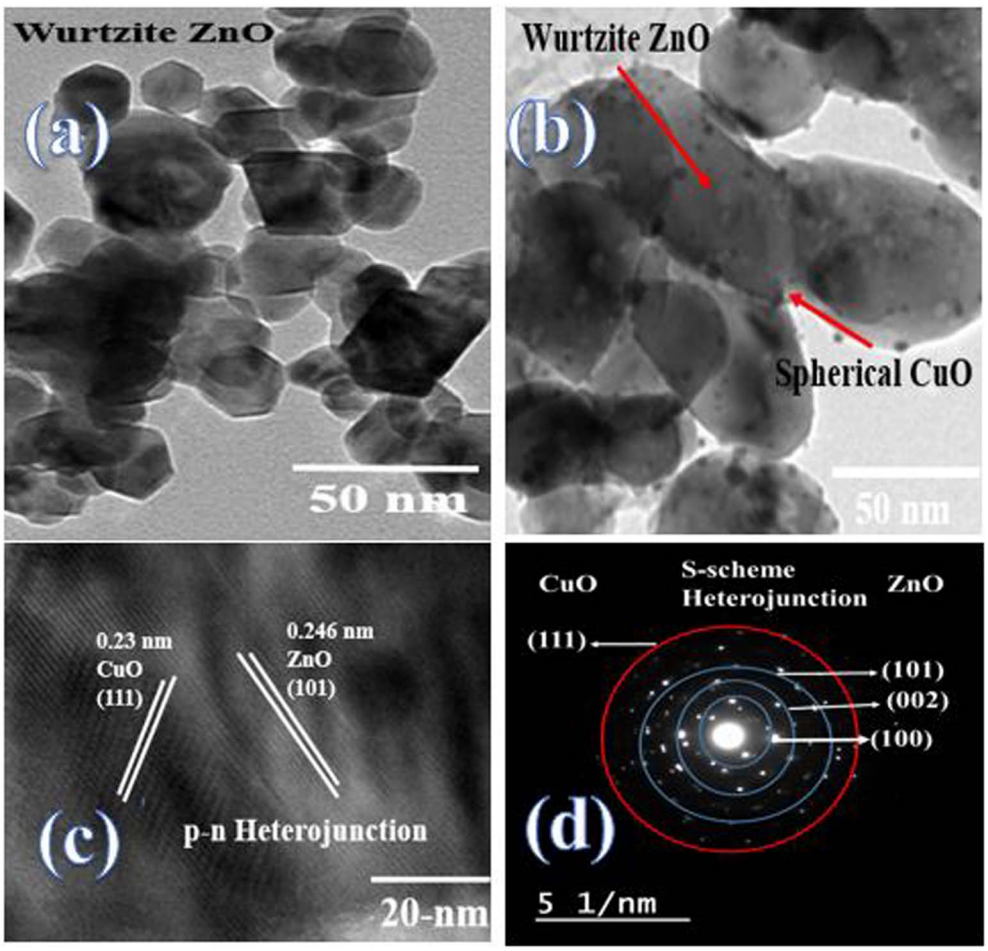

Fig. 3 HRTEM of (a) ZnO and (b) ZnCu10, (c) line space in ZnCu10 and (d) SAED of ZnCu10.

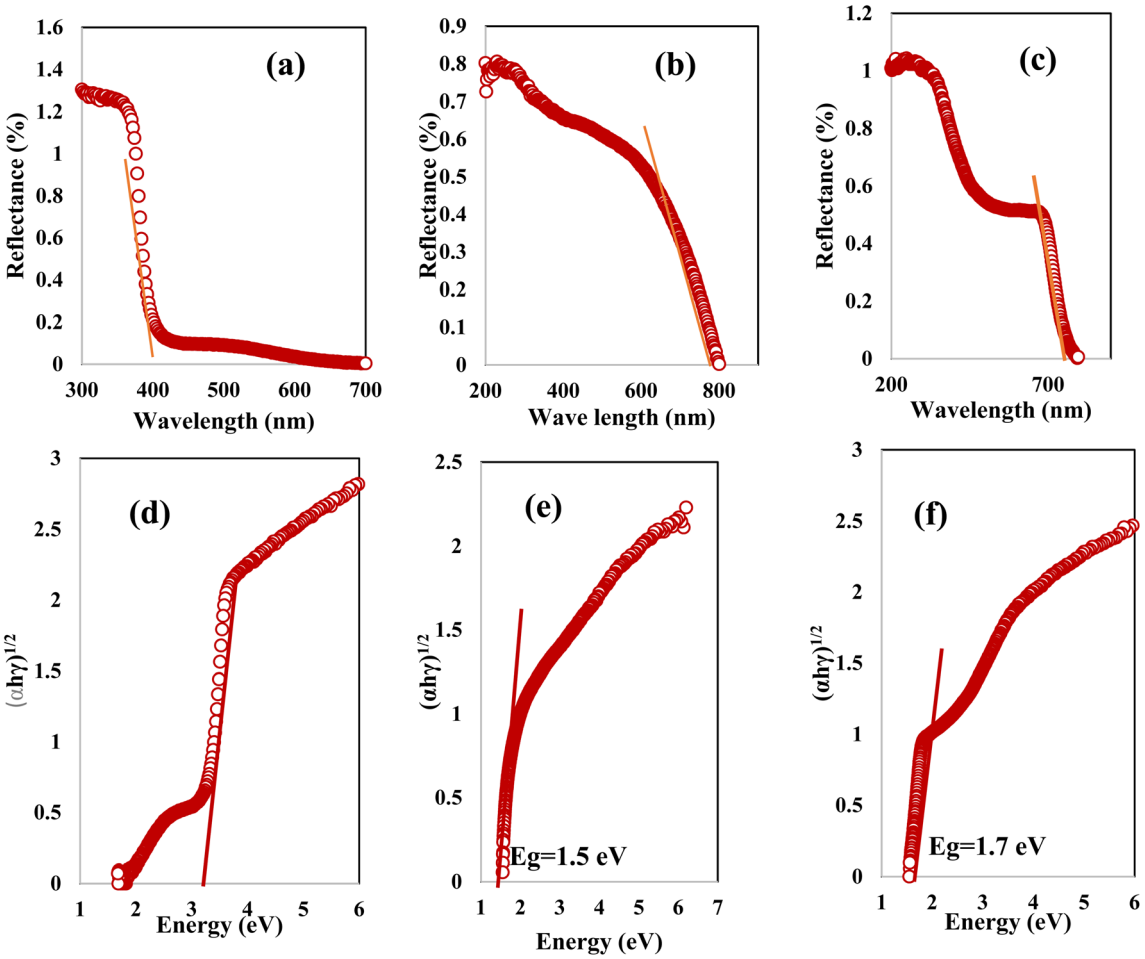

Fig. 4 DRS of (a) ZnO, (b) CuO, and (c) ZnCu10, and Tauc plot of (d) ZnO, (e) CuO and (f) ZnCu10.

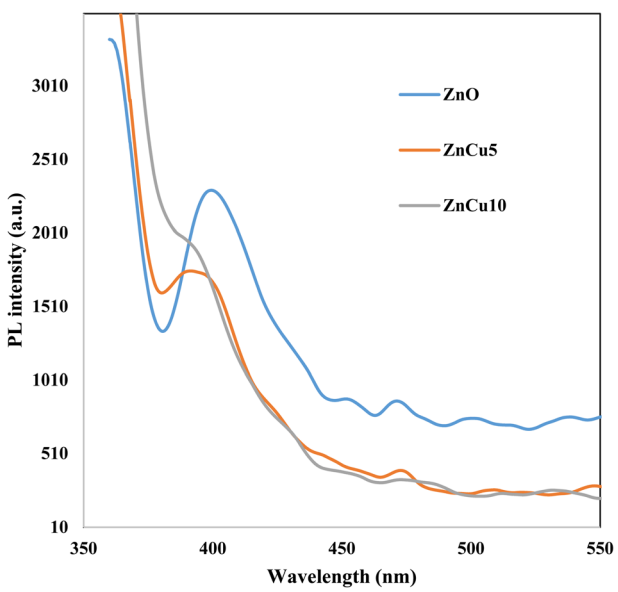

Fig. 5 PL spectrum of ZnO, ZnCu5 and ZnCu10.

[Fig. 7b]. The kinetic plot indicates that the photocatalytic rate constant of RhB dye decomposition on the surface of the ZnCu10 heterojunction is twenty-fold faster than that of pristine ZnO [Fig. 7c]. The nature of reactive oxygen species and hot electron–hole pairs is examined under visible radiation to shed light on the mechanism of electron–hole transportation in the circuit of CuO/ZnO heterojunctions. 1×10^{-3} M concentration of benzoquinone aqueous solution is introduced in a mixture of RhB dye and 0.1 g of the photocatalyst as an efficient scrubber for trapping superoxide radicals. Benzoquinone depressed the decomposition rate of RhB dye, directing the attention to the impulsive role of reactive oxygen species in mineralizing the toxic dye solution [Fig. 8a]. The PL spectrum of terephthalic acid under solar light irradiation follows up the production of hydroxyl radicals from water oxidation by valence band hot holes produced on either the ZnO or CuO surface. On examining Fig. 8b–d, one can notice the production of a well-defined PL signal of hydroxyl terephthalic acid on ZnO and ZnCu10 nanoparticles. On the contrary, the poor signal recorded in the PL spectrum of terephthalic acid on the CuO surface reveals the weak production of hydroxyl radicals. These results manifest that hydroxyl radicals are generated from oxidation of water on the ZnO surface as the oxidative photocatalyst; however, CuO

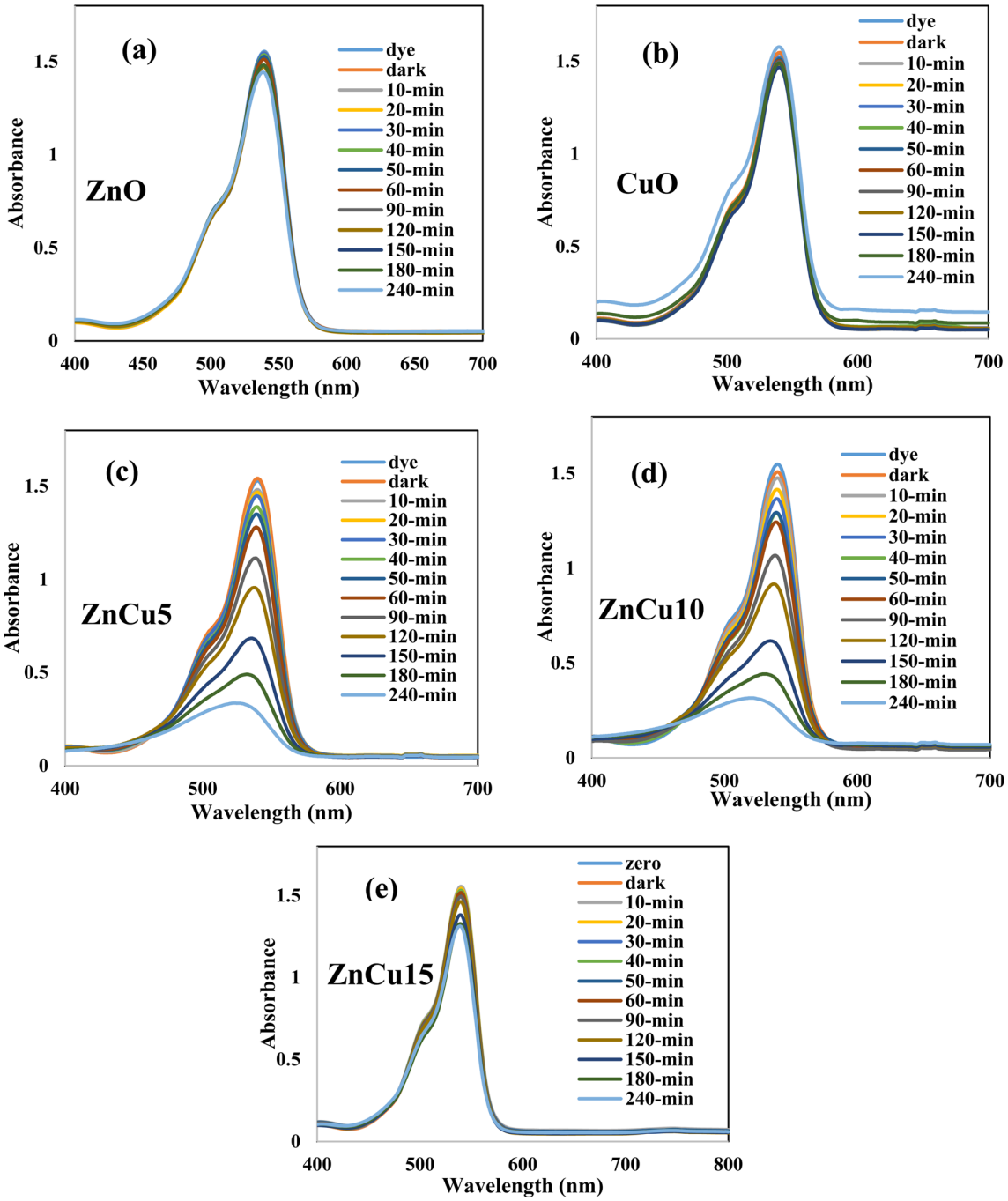

Fig. 6 The absorption spectrum of photocatalytic degradation of rhodamine B dye over the surface of (a) ZnO, (b) CuO, (c) ZnCu5, (d) ZnCu10 and (e) ZnCu15.

plays a role of a reductive photocatalyst in the heterojunction circuit. Total organic carbon [TOC], which is the actual measurement of decomposition of RhB dye molecules, is reduced from 79.1 mg L^{-1} to 7.4 mg L^{-1} on the surface of the ZnCu10 heterojunction, revealing the degradation of RhB dye into eco-friendly species.

The charge transportation between two semiconductors is explained by various mechanisms. Type II, Z-scheme and S-scheme mechanisms are the popular routes for describing the charge migration between two different semiconductors. The staggered type II heterojunction is unfavorable from dynamic, thermodynamic and energetic points of view. Through the type II heterojunction, electrons migrate from high to low conduction band and holes jump from low to high valence band. This charge transportation depresses the redox efficiency of the charge carriers. All types of Z-scheme cannot explain, with precise analysis, the actual mechanism of charge transportation. Recently, the S-scheme heterojunction is vividly

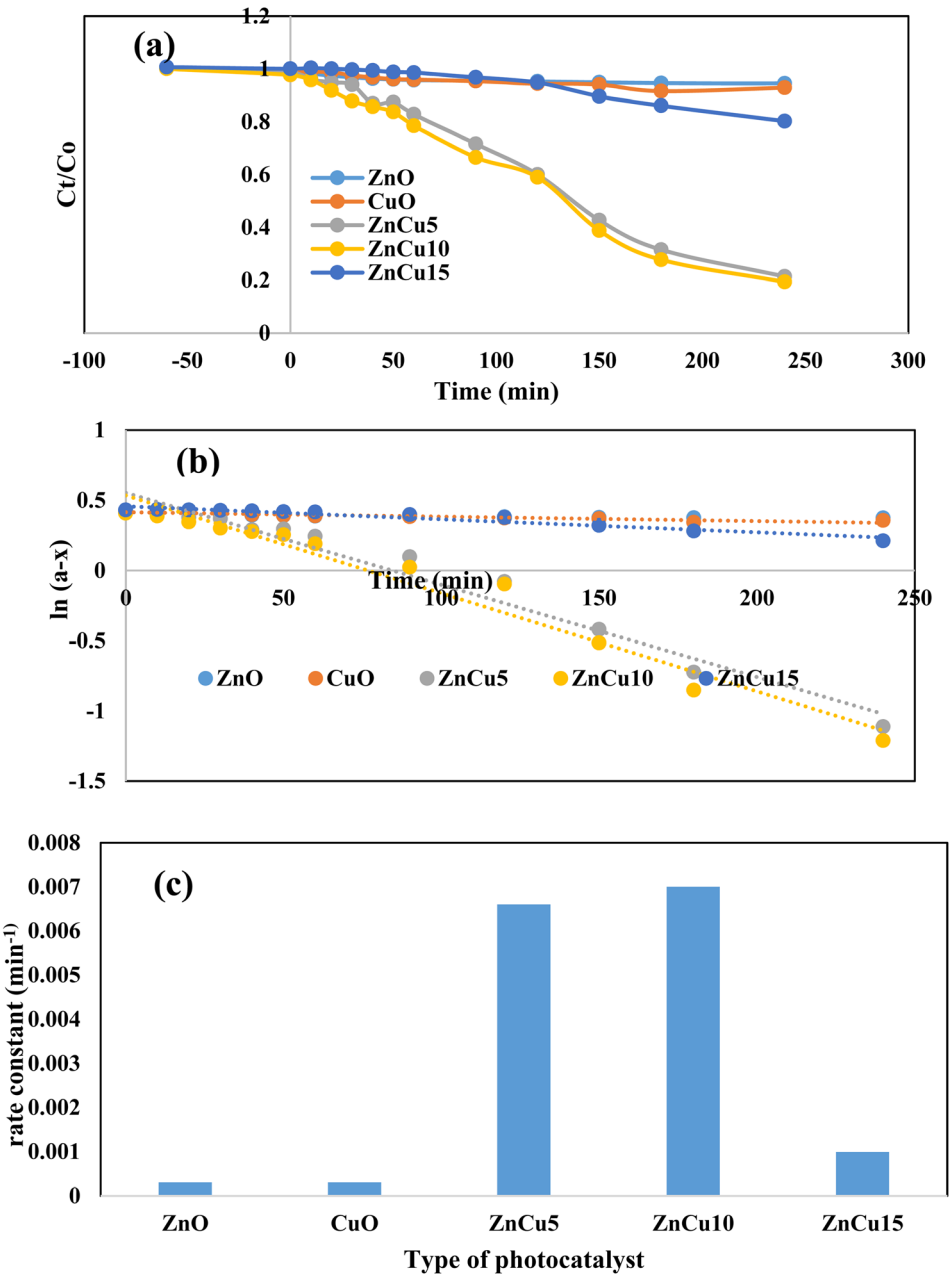

Fig. 7 (a) The variation of removal of RhB dye with time of irradiation on the surface of ZnO, CuO, ZnCu5, ZnCu10 and ZnCu15, (b) pseudo-first order plot of photocatalytic degradation of RhB dye on the surface of ZnO, CuO, ZnCu5, ZnCu10 and ZnCu15, and (c) the effect of the change in concentration of the photocatalyst with pseudo first order rate constant of photocatalytic degradation of RhB dye.

a more precise route for predicting the charge transfer progress between two different semiconductors under light illumination. The S-scheme heterojunction is usually composed of two semiconductors of different redox potential. The universal parameter requires that the Fermi level and conduction band position of the reductive photocatalyst be higher than those of the oxidative photocatalyst. Concurrently, the work function of the oxidative photocatalyst should be higher than that of the reductive photocatalyst. The work functions reported in the previous literature research of ZnO and CuO nanoparticles are 5.17 eV and ~2.5 eV, respectively.[53–55] Accordingly, ZnO acts as an oxidative photocatalyst and CuO is a reductive photocatalyst. The reported values of the conduction band for CuO and ZnO are approximately −0.92 and −0.27 eV, respectively.[43,44,52,57] Likewise, the valence band potentials of ZnO and CuO are positioned at 2.78 and 0.28 eV, respectively.[43,44,52,57] As represented in Fig. 9, the Fermi level and the conduction band of CuO are higher than those of ZnO. On hybridizing ZnO with CuO sonochemically, electrons transfer from CuO to ZnO, creating a positive charge on the CuO side and negative charge

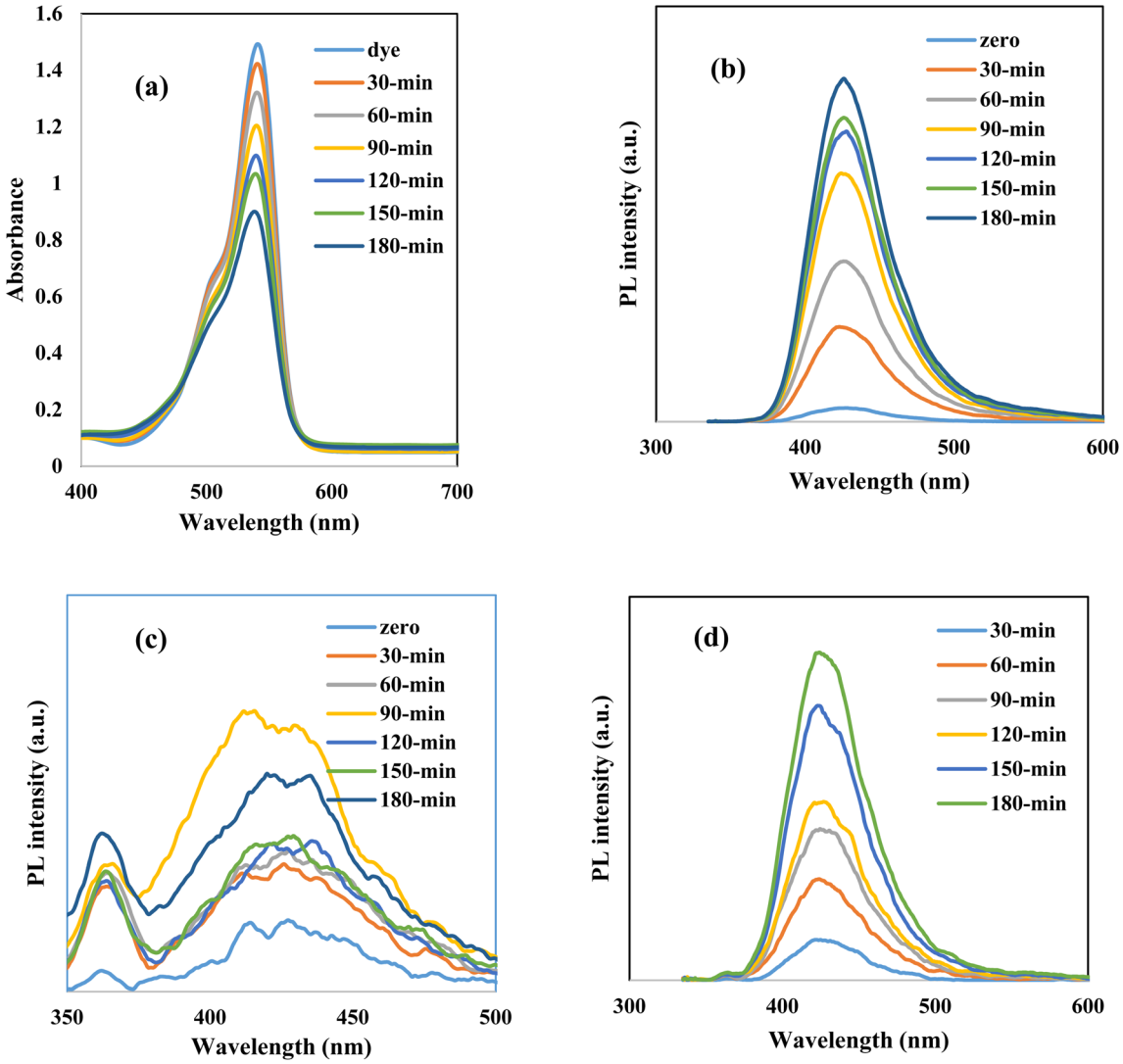

Fig. 8 (a) The spectrum of the photocatalytic degradation of RhB in the presence of 10^{-3} M benzoquinone on the surface of ZnCu10, (b) PL spectrum of terephthalic acid on ZnO, (c) PL spectrum of terephthalic acid on CuO and (d) PL spectrum of terephthalic acid on ZnCu10.

on the ZnO side. This charge transfer generates an accumulation layer on the ZnO side and a depletion layer on the CuO side. Concurrently, the Fermi levels of ZnO and CuO bend upward and downward until the two Fermi levels are equalized [Fig. 9]. At this point, an internal electric field directed from CuO to ZnO accelerates the electron transfer from the oxidative to reductive photocatalyst. Upon light irradiation, the electrons are derived from the conduction band of ZnO to the valence band of CuO to vanish through the coulombic attraction force. On other hand the positive holes in the valence band of ZnO (E_{VB} = +2.8 eV) and electrons in the conduction band of CuO (E_{CB} = −0.92 eV) are available for consumption in the photocatalytic reaction. The mechanism of the charge transportation during photocatalytic reactions is also verified according to the radical scavenging results and PL spectrum of terephthalic acid. The valence band potential of ZnO is more positive than the oxidation potential of water ($E_{OH/OH.}$ = +2.4 eV),[56] generating a huge amount of hydroxyl radicals, as proved from PL emission of terephthalic acid. Moreover, the conduction band potential of CuO is more negative than the reduction potential of water (E_{O_2/O_2} = −0.34 eV), accounting for the production of superoxide radicals as confirmed from benzoquinone trapping experiments.[56] The production of reactive oxygen species on the photocatalyst surface implies the successful production of an S-scheme CuO/ZnO heterojunction with strong redox power for destructing organic dyes. Table 1 illustrates a comparative study for RhB removal on CuO/ZnO nanoparticles synthesized in our research and those reported in the previous research.[43–51] The literature data collected in Table 1 reveal that our as-synthesized heterojunction is efficient in decomposing RhB dye under solar radiation through simple operating conditions without requiring a complicated mode of preparation that requires high cost and more energy suppliers as reported in the previous research.

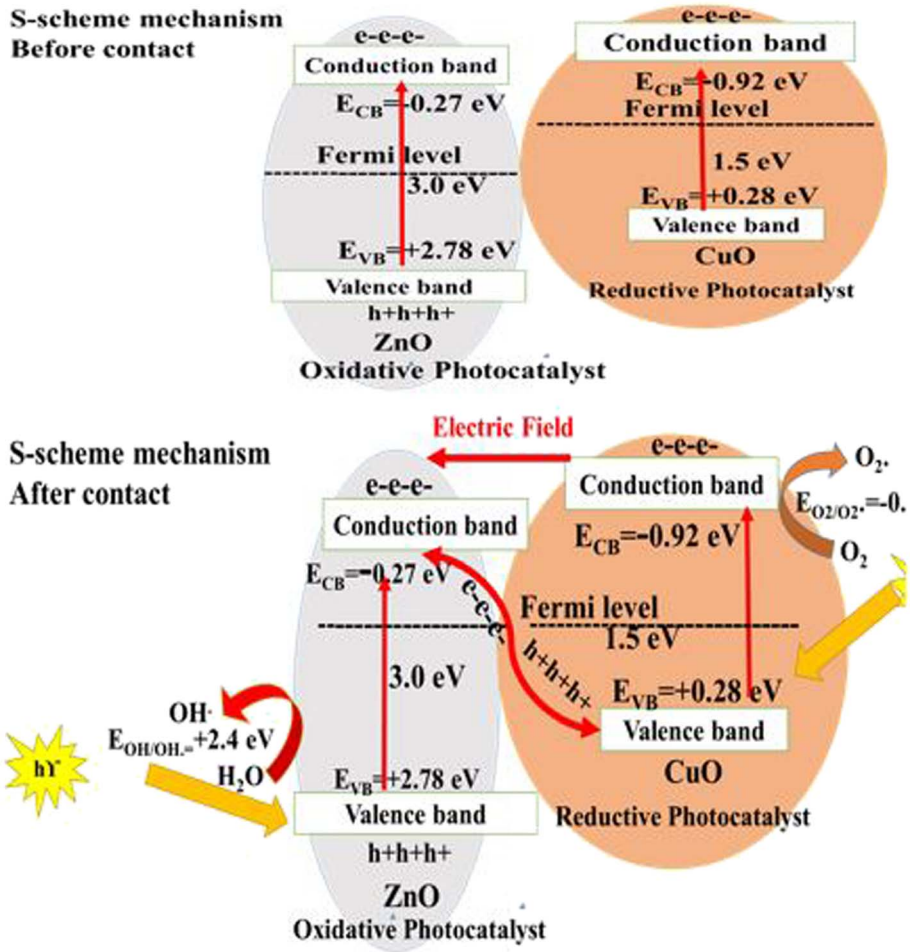

Fig. 9 S-scheme charge transportation mechanism between ZnO and CuO before and after contact.

Table 1 Comparative study of removal of organic dyes on CuO/ZnO nanoparticles

Photocatalyst	Mode of preparation	Organic dye	Light source	Degradation (%)	Reference
CuO/ZnO	Sonochemical	Rhodamine B	Visible light	95%	Our research
Ag/CuO/ZnO	Co-precipitation	Methylene blue	Metal halide lamp	95%	43
ZnO/CuO	Microwave	Acid orange 7	250W Xe lamp	80%	44
ZnO/CuO/MoO_3	Hydrothermal	Rhodamine B	300 W Xe lamp	90%	45
CuO/ZnO	Thermal oxidation	Methylene blue	300 W Xe lamp	92%	46
CuO/ZnO	Green biosynthesis	Methylene blue	500 W tungsten halogen	94%	47
CuO/ZnO	Impregnation	Methylene blue	400 W UV lamp	95%	48
CuO/ZnO	Hydrothermal	Methylene blue	500 W halogen lamp	96%	49
CuO/ZnO	Hydrothermal	Rhodamine 6G	Sun light	40%	50
Ag/CuO–ZnO	Hydrothermal-chemical reduction	Rhodamine 6G	Sun light	95%	50
CuO/ZnO	Thermal oxidation	Rhodamine B	Xenon lamp	92%	51

4. Conclusions

In this novel research work, an S-scheme heterojunction is successfully generated sonochemically by hybridizing a ZnO oxidative photocatalyst and CuO reductive photocatalyst. The novel sonicated CuO/ZnO heterojunction promotes the charge separation and transportation and prohibits the photocatalytic reaction with charge carriers with strong redox potential. The co-existence of ZnO and CuO diffraction peaks, reduced band gap energy, depression in the PL signal and production of reactive oxygen species manifest the successful production of an S-scheme heterojunction. The heterojunction containing 10 wt% CuO and 90 wt% ZnO degraded 93% of RhB dye under solar irradiation. The PL spectrum analysis of terephthalic acid

reveals the production of hydroxyl radicals by oxidation of water by the hot holes of ZnO. However, superoxide radicals are produced from water reduction by the hot electrons of the CuO conduction band. The novel heterojunction is considered a potential photocatalyst for expelling organic dyes from wastewater under solar radiation.

Conflicts of interest

There are no conflicts to declare.

Acknowledgements

We are grateful for the financial supported by Researchers Supporting Project number (RSP2023R78), King Saud University, Riyadh, Saudi Arabia.

References

1 M. A. Ahmed and Z. M. Abou-Gamra, Mesoporous MgO nanoparticles as a potential sorbent for removal of fast orange and bromophenol dyes, *Nanotechnol. Environ. Eng.*, 2016, **1**(10), 2–11.

2 M. Adel, M. A. Ahmed and A. A. Mohamed, Effective removal of cationic dyes from aqueous solution using reduced graphene oxide functionalized with manganese ferrite nanoparticles Composites, *Commun.*, 2020, **22**, 100450.

3 M. Adel, M. A. Ahmed, M. Adel, M. A. Ahmed and A. A. Mohamed, Synthesis and characterization of magnetically separable and recyclable crumbled $MgFe_2O_4$/reduced graphene oxide nanoparticles for removal of methylene blue dye from aqueous solutions, *J. Phys. Chem. Solid*, 2021, **149**, 109760.

4 M. Adel, M. A. Ahmed and A. A. Mohamed, A facile and rapid removal of cationic dyes using hierarchically porous reduced graphene oxide decorated with manganese ferrite, *Flat Chem.*, 2021, **26**, 100233.

5 M. Adel, M. A. Ahmed, M. A. Elabiad and A. A. Mohamed, Removal of heavy metals and dyes from wastewater using graphene oxide-based nanomaterials: A critical review, *Environ. Nanotechnol. Monitor. Manag.*, 2022, **18**, 100719.

6 M. A. Ahmed, A. Fahmy, M. G. Abo-Zaed and E. M. Hashem, Fabrication of novel $AgIO_4/SnO_2$ heterojunction for photocatalytic hydrogen production through direct Z-scheme mechanism, *J. Photochem. Photobiol., C*, 2020, **400**, 112660.

7 Z. M. Abou-Gamra, M. A. Ahmed and M. A. Hamza, Investigation of commercial $PbCrO_4/TiO_2$ for photodegradation of rhodamine B in aqueous solution by visible light, *Nanotechnol. Environ. Eng.*, 2017, **2**, 12.

8 M. Abd Elnaby Wafi, M. A. Ahmed, H. S. Abdel-Samad and H. A. A. Medien, Exceptional removal of methylene blue and p-aminophenol dye over novel TiO_2/RGO nanocomposites by tandem adsorption-photocatalytic processes, *Mater. Sci. Energy Technol.*, 2022, **5**, 217–231.

9 M. A. Ahmed, M. F. Abdel-Messih and E. H. Ismail, Facile synthesis of novel microporous $CdSe/SiO_2$ nanocomposites selective for removal of methylene blue dye by tandem adsorption and photocatalytic process, *J. Mater. Sci.: Mater. Electron.*, 2019, **30**, 17527–17539.

10 M. A. Alshakhanbeh, M. A. Ahmed, Z. M. Abou-Gamra and H. Madien, Influence of dispersion of various proportions of metallic gold nanoparticles on the optical and photocatalytic properties of titania, *Mater. Sci. Energy Technol.*, 2020, **3**, 429–439.

11 M. A. Ahmed, N. Al-Zaqri, A. Ali, A. H. Glal and E. Mahmood, Rapid photocatalytic degradation of RhB dye and photocatalytic hydrogen production on novel curcumin/SnO_2 nanocomposites through direct Z-scheme mechanism, *J. Mater. Sci. Mater. In electronics*, 2020, **31**(21), 19188–19203.

12 E.-H. Hashem, A. Fahmy, A. Abbas, M. Tarek, B. Mahran and M. A. Ahmed, Fabrication of novel $AgIO_4/TiO_2$ heterojunction for photocatalytic hydrogen production through direct Z-scheme mechanism, *Nanotechnol. Environ. Eng.*, 2020, **5**, 17.

13 Y. Zhang, G. Ma. Wang, B. Ma and Z. Jin, CdS pen heterojunction co-boosting with Co_3O_4 and Ni-MOF-74 for photocatalytic hydrogen evolution, *Dalton Trans.*, 2018, **47**, 1176–1180.

14 A. Ali, A. H. Galal, E. F. El-Sherbeny, A. Soltan, M. F. Abdel-Messih and M. A. Ahmed, Fabrication of S-scheme TiO_2/g-C_3N_4 nanocomposites for generation hydrogen gas and removal of fluorescein dye, *Diamond Relat. Mater.*, 2022, **122**, 108819.

15 L. Jing, D. Wang, Y. Xu, M. Xie, J. Yan, M. He, Z. Song, H. Xu and H. Li, Porous defective carbon nitride obtained by a universal method for photocatalytic hydrogen production from water splitting, *J. Colloid Interface Sci.*, 2020, **566**, 171–182.

16 A. Alsalme, A. AlFawaz, A. H. Glal, M. F. Abdel Messih, A. Soltan and M. A. Ahmed, S-scheme $AgIO_4/CeO_2$ heterojunction nanocomposite photocatalyst for degradation of rhodamine B dye, *J. Photochem. Photobiol., C*, 2023, **439**, 114596.

17 Y. Xiao, H. Yu and X. Dong, Ordered mesoporous CeO_2/ZnO composite with photodegradation concomitant photocatalytic hydrogen production performance, *J. Solid State*, 2019, **278**, 120893.

18 M. F. Abdel Messih, M. A. Ahmed, A. Soltan and S. S. Anis, Synthesis and characterization of novel Ag/ZnO nanoparticles for photocatalytic degradation of methylene blue under UV and solar irradiation, *J. Phys. Chem. Solids*, 2019, **135**, 109086.

19 M. S. Hamdy, H. S. M. Abd-Rabboh, M. Beneissa, M. Gad Al-Metwaly, A. H. Glal and M. A. Ahmed, Fabrication of novel polyaniline/ZnO heterojunction for exceptional photocatalytic hydrogen production and degradation of fluorescein dye through direct Z-scheme mechanism, *Opt. Mater.*, 2021, **117**, 111198.

20 E. M. Ezz el-regal, M. A. Ahmed, M. F. Abdel-Messih and Z. M. Abou-Gamra, Synthesis of novel ZnO nanoparticles with exceptional crystalline and photocatalytic features

toward recalcitrant pollutant: Fluorescein dye, *Opt. Mater.*, 2021, **111**, 110597.

21 A. H. Galal, M. G. Elmahgary and M. A. Ahmed, Construction of novel AgIO4/ZnO/graphene direct Z-scheme heterojunctions for exceptional photocatalytic hydrogen gas production, *Nanotechnol. Environ. Eng.*, 2021, **6**(1), 5.

22 M. F. Abdel Messih, A. E. Shalan, M. F. Sanad and M. A. Ahmed, Facile approach to prepare ZnO@SiO_2 nanomaterials for photocatalytic degradation of some organic pollutant models, *J. Mater. Sci.*, 2019, **30**, 1491–1499.

23 R. Abdel-Aziz, M. A. Ahmed and M. F. Abdel-Messih, A novel UV and visible light driven photocatalyst $AgIO_4$/ZnO nanoparticles with highly enhanced photocatalytic performance for removal of rhodamine B and indigo carmine dye, *J. Photochem. Photobiol., A*, 2020, **389**, 112245.

24 S. Sharma, S. Singh and N. Khare, Enhanced photosensitization of zinc oxide nanorods using CuO for efficient photocatalytic and photoelectrochemical water splitting, *Int. J. Hydrogen Energy*, 2016, **41**, 21088–21098.

25 R. Saravanan, E. Sacari, F. Gracia, M. M. Khan, E. Mosquera and V. K. Gupta, Conducting PANI stimulated ZnO system for visible light photocatalytic degradation of coloured dyes, *J. Mol. Liq.*, 2016, **221**, 1029–1033.

26 V. Eskizeybek, F. Sarı, H. Gülce, A. Gulce and A. Avcı, Preparation of the new CuO/ZnO nanocomposite and its photocatalytic activity for degradation of methylene blue and malachite green dyes under UV and natural sun lights irradiations, *Appl. Catal., B*, 2012, **5**, 197–206.

27 J. Zhu, C. Shao, X. Li, C. Han, S. Yang, J. Ma, X. Li and Y. Liu, Immobilization of ZnO/CuO heterojunction on electrospun polyacrylonitrile nanofibers and enhanced photocatalytic activity, *Mater. Chem. Phys.*, 2018, **214**, 507–515.

28 C. Li, X. Liu, X. Yang, T. Peng, Y. Li, M. Chen, C. Lin, J. Jiang, Z. Su, W. Kong and Y. Wang, Tetragonal multilayered ZnO/CuO composites derived from Zn- and Cu-containing metal-organic framework: Effect of calcination temperature on physicochemical properties and photocatalytic activity Tetragonal multilayered ZnO/CuO composites derived from Zn- and Cu-containing metal-organic framework: Effect of calcination temperature on physicochemical properties and photocatalytic activity, *Ceram. Interfaces*, 2022, **48**, 18467.

29 Y. Wu, D. Meng, Q. Guo, D. Gao and L. Wang, Study on TiO_2/g-C_3N_4 S-Scheme heterojunction photocatalyst for enhanced formaldehyde decomposition, *Opt. Mater.*, 2022, **126**, 112213.

30 Q. Xu, L. Zhang, B. Cheng, J. Fan and J. Yu, S-Scheme Heterojunction Photocatalyst, *Chem*, 2020, **6**, 1543–1559.

31 S. Wageh, A. A. Al-Ghamdi, R. J. X. Li and P. Zhang, A new heterojunction in photocatalysis: S-scheme heterojunction, *Chin. J. Catal.*, 2021, **42**, 667–669.

32 L. Zhang, J. Zhang, H. Yu and J. Yu, Emerging S-Scheme Photocatalyst, *Adv. Mater.*, 2022, **34**, 2107668.

33 A. Meng, B. Cheng, H. Tan, J. Fan, C. Su and J. Yu, TiO_2/polydopamine S-scheme heterojunction photocatalyst with enhanced CO_2-reduction selectivity, *Appl. Catal. Environ.*, 2021, **289**, 120039.

34 Y. Xiao, Z. Ji, C. Zou, Yi. Xu, R. Wang, J. Wu, G. Liu, P. He, Q. Wang and T. Jia, Construction of CeO_2/BiOI S-scheme heterojunction for photocatalytic removal of elemental mercury, *Appl. Surf. Sci.*, 2021, **556**, 149767.

35 H. Ge, F. Xu, B. Cheng, J. Yu and W. Ho, S-scheme heterojunction TiO_2/CdS Nanocomposites fibers as H_2-production photocatalyst, *Chem. Cat. Chem.*, 2019, **11**, 6301–6309.

36 Q. Li, W. Zhao, Z. Zhai, K. Ren, T. Wang, H. Guan and H. Shi, 2D/2D Bi_2MoO_6/g-C_3N_4 S-scheme heterojunction photocatalyst with enhanced visible-light activity by Au loading, *J. Mater. Sci. Technol.*, 2020, **56**, 216–226.

37 S. Jiang, J. Cao, M. Guo, D. Cao, X. Jia, H. Lin and S. Chen, Novel S-scheme WO_3/RP composite with outstanding overall water splitting activity for H_2 and O_2 evolution under visible light, *Appl. Surf. Sci.*, 2021, **558**, 149882.

38 X. Zhang, Y. Zhang, X. Jia, N. Zhang, R. Xia, X. Zhang, Z. Wang and M. Yu, In situ fabrication of a novel S-scheme heterojunction photocatalyts Bi_2O_3/P-C_3N_4 to enhance levofloxacin removal from water, *Sep. Purif. Technol.*, 2021, **268**, 118691.

39 Q. Liu, X. He, J. Peng, X. Yu, H. Tang and J. Zhang, Hot-electron-assisted S-scheme heterojunction of tungsten oxide/graphitic carbon nitride for broad-spectrum photocatalytic H_2 generation, *Chin. J. Catal.*, 2021, **42**, 1478–1487.

40 K. Zhang, D. Li, Q. Tian, H. Cao, F. Orudzhev, I. A. Zvereva, J. Xu and C. Wang, Recyclable 0D/2D $ZnFe_2O_4$/$Bi_5FeTi_3O_{15}$ S-scheme heterojunction with bismuth decoration for enhanced visible-light-driven tetracycline photodegradation, *Ceram. Interfaces*, 2021, **47**, 17109–17119.

41 S. Wu, X. Yu, J. Zhang, Y. Zhang, Y. Zhu and M. Zhu, Construction of BiOCl/$CuBi_2O_4$ S-scheme heterojunction with oxygen vacancy for enhanced photocatalytic diclofenac degradation and nitric oxide removal, *Chem. Eng. J.*, 2021, **411**, 128555.

42 V. V. Pham, D. Q. Mai, D. P. Bui, T. V. Man, B. Zhu, L. Zhang, J. Sangkaworn, J. Tantirungrotechai, V. Reutrakul and T. M. Cao, Emerging 2D/0D g-C_3N_4/SnO_2 S-scheme photocatalyst: new generation architectural structure of heterojunctions toward visible-light-driven NO degradation, *Environ. Pollut.*, 2021, **286**, 117510.

43 A. Zare, A. Saadati and S. Sheibani, Modification of a Z-scheme ZnO-CuO nanocomposite by Ag loading as a highly efficient visible light photocatalyst, *Mater. Res. Bull.*, 2023, **158**, 112048.

44 S. Ruan, W. Huang, M. Zhao, H. Song and Z. Gao, A Z-scheme mechanism of the novel ZnO/CuO n-n heterojunction for photocatalytic degradation of Acid Orange 7, *Mater. Sci. Semicond. Process.*, 2020, **107**, 104835.

45 M. K. Hussain, N. R. Khalid, M. B. Tahir, M. Tanveer, T. Iqbal and M. Liaqat, Enhanced visible light-driven photocatalytic activity and stability of novel ternary ZnO/CuO/MoO_3 nanorods for the degradation of rhodamine B and alizarin yellow, *Maters. Sci. Semiconductor Process*, 2023, **155**, 107261.

46 X. Wang, M. Deng, Z. Zhao, Q. Zhang and Y. Wang, Synthesis of super-hydrophobic CuO/ZnO layered composite nano-photocatalyst, *Mater. Chem. Phys.*, 2022, **276**, 125305.

47 A. Fouda, S. S. Salem, A. R. Wassel, M. F. Hamza and T. Shaheen, Optimization of green biosynthesized visible light active CuO/ZnO nano-photocatalysts for the degradation of organic methylene blue dye, *Heliyon*, 2020, **6**, 04896.

48 A. G. Acedo-Mendoza, A. Infantes-Molina, D. Vargas-Hernandez, C. A. Chavez-Sanchez, E. Rodríguez-Castellon and J. C. Tanori-Cordova, Photodegradation of methylene blue and methyl orange with CuO supported on ZnO photocatalysts: The effect of copper loading and reaction temperature, *Maters. Sci. Semiconductor Process.*, 2020, **119**, 105257.

49 S. Harish, J. Archana, M. Sabarinathan, M. Navaneethan, K. D. Nisha and S. Ponnusamy, Controlled structural and compositional characteristic of visible light active ZnO/CuO photocatalyst for the degradation of organic pollutant, *Appl. Surf. Sci.*, 2017, **418**, 103–112.

50 J. Singh and R. K. Soni, Efficient charge separation in Ag nanoparticles functionalized ZnO nanoflakes/CuO nanoflowers hybrids for improved photocatalytic and SERS activity, *Colloids Surf.*, 2021, **626**, 127005.

51 Fa Cao, T. Wang and X. Ji, Enhanced visible photocatalytic activity of tree-like ZnO/CuO nanostructure on Cu foam, *Appl. Surf. Sci.*, 2019, **471**, 417–424.

52 W. T. Alsaggaf, A. Shawky and M. H. H. Mahmoud, S-scheme CuO/ZnO p–n heterojunctions for endorsed photocatalytic reduction of mercuric ions under visible light, *Inorg. Chem. Commun.*, 2022, **143**, 109778.

53 D. Barman, J. Borah, S. Deb and B. K. Sarma, Design strategy for CuO-ZnO S-scheme heterojunction photocatalysts in the presence of plasmonic Ag and insights into photoexcited carrier generation and interfacial transfer in diverse structural configurations of the heterostructure system, *Colloids Surf., A.*, 2023, **663**, 131077.

54 J. Yan, P. Xu, S. Chen, G. Wang, F. Zhang, W. Zhao, Z. Zhang, Z. Deng, M. Xu, J. Yun and Y. Zhang, Construction of highly ordered ZnO microrod@SnO_2 nanowire heterojunction hybrid with a test-tube brush-like structure for high performance lithium-ion batteries: experimental and theoretical study, *Electrochim. Acta*, 2020, **330**, 135312.

55 Y. W. Zhu, T. Yu, F. C. Cheong, X. J. Xu, C. T. Lim, V. B. C. Tan, J. T. L. Thong and C. H. Sow, Large-scale synthesis and field emission properties of vertically oriented CuO nanowire films, *Nanotechnology*, 2005, **16**, 88–92.

56 D. Huang, S. Chen, G. Zeng, X. Gong, C. Zhou, M. Cheng, W. Xue, X. Yan and J. Li, Artificial Z-scheme photocatalytic system: what have been done and where to go?, *Coord. Chem. Rev.*, 2019, **385**, 44–80.

57 C. Li, X. Liu, X. Yang, T. Peng, Y. Li, M. Chen, C. Lin, J. Jiang, Z. Su, W. Kong and Y. Wang, Tetragonal multilayered ZnO/CuO composites derived from Zn- and Cu-containing metal-organic framework: effect of calcination temperature on physicochemical properties and photocatalytic activity, *Ceram. Interfaces*, 2022, **48**, 18460.